Tailoring the Electronic and Magnetic Properties of Hematene by Surface Passivation: Insights from First-principles Calculations

Wei, Y.; Ghorbani Asl, M.; Krasheninnikov, A.;

Originally published:

September 2020

Journal of Physical Chemistry C 124(2020)41, 22784-22792

DOI: https://doi.org/10.1021/acs.jpcc.0c05807

Tailoring the electronic and magnetic properties of hematene by surface passivation: insights from first-principles calculations

Yidan Wei, Mahdi Ghorbani-Asl, and Arkady V. Krasheninnikov*

ABSTRACT

Exfoliation of atomically-thin layers from non-van der Waals bulk solids gave rise to the emergence of a new class of two-dimensional (2D) materials, such as hematene (Hm), a structure just a few atoms thick obtained from hematite. Due to a large number of unsaturated sites, Hm surface can be passivated under ambient conditions. Using density functional theory calculations, we investigate the effects of surface passivation with H and OH groups on Hm properties and demonstrate that the passivated surfaces are energetically favorable under oxygen-rich conditions. While the bare sheet is antiferromagnetic and possesses an indirect band gap of 0.93 eV, the hydrogenated sheets are half-metallic with a ferromagnetic ground state, and the fully hydroxylated sheets are antiferromagnetic with a larger band gap as compared to the bare system. The electronic structure of Hm can be further tuned by mechanical deformations. The band gap of fully passivated Hm increases monotonically with biaxial strain, hinting at potential applications of Hm in electromechanical devices.

Email: mahdi.ghorbani@hzdr.de

1. INTRODUCTION

Two-dimensional (2D) materials typically have bulk counterparts, which possess a layered structure with strong covalent bonds within the planes, and weak van der Waals (vdW) bonds between the layers.[1] This makes mechanical or chemical exfoliation of single layers from the bulk material possible.[2,3] However, it also indicates that exfoliation of stable monolayers from nonlayered crystals is extremely challenging due to the absence of the anisotropy in the bonding and high surface energies.

Surprisingly, several 2D materials were recently manufactured from metal ores, which are non-vdW solids.[4–7] Among them, hematene (Hm), an atomically thin structure obtained from bulk α-Fe_2O_3, or hematite (Ht), has attracted particular attention due to its exceptional magnetic and electronic properties in comparison to its bulk counterpart.[4,5] Following the exfoliation of Hm, other 2D compounds have been successfully exfoliated from earth-abundant non-layered materials such as ilmenite, goethite or calcite.[6,7] These materials comprise a new class of non-vdW 2D systems. The large-scale production of the non-vdW 2D materials is still in its infancy, though, since it requires precise control over the crystalline orientations, lateral size and chemical termination of the fabricated materials.

Magnetic layered materials in the bulk form usually display intrinsic magnetic anisotropy due to their reduced symmetry.[8] Nevertheless, preserving the magnetic character while reducing the thickness to a single layer is a challenging task. The previous experimental results claimed the ferromagnetic order in Hm contrary to the antiferromagnetic ground state of the bulk material Ht.[4] However, the results of recent density functional theory (DFT) calculations[5,9] indicated that

antiferromagnetic ordering in the bulk phase is preserved in the 2D limit. This discrepancy was explained by considering the chemical bonding between Fe atoms in the Hm layer to the substrate which turns Hm into a 2D ferrimagnet.

Exfoliation of the bulk material down to the atomically-thin sheets modifies its physical properties due to the quantum confinement, which provides exciting opportunities for various applications.[10] In the case of non-vdW nanomaterials, the exfoliated samples also enable new functionalities originating from the unsaturated sites that are absent in the typical vdW 2D materials. For example, it is shown that such non-vdW 2D materials possess superior electrocatalytic reactivity due to the high density of surface-active sites on their basal plane and modified electronic structure.[7,11] However, the main problem is their low structural stability and rapid degradation under ambient conditions. To this end, the passivation of the surface with functional groups is an effective way to preserve the stability and reliability of non-vdW 2D materials in the fabricated devices.[12] In addition, the experimental exfoliation process is typically performed in a solvent, which leads to the passivation of dangling bonds.

In this context, an important question to be answered is how the electronic and magnetic properties of the cleaved sheet change upon surface passivation. Atomistic simulations at the DFT level can provide lots of insight into the effects of passivation. At the same time, although a few studies have been performed to examine the structural and electronic properties of Hm, there is no theoretical study on the physicochemical properties of Hm nanosheets, which would systematically address the effects of surface passivation by most probable atoms and functional groups. In addition, it is known that the electronic and optical properties of 2D materials are extremely sensitive to lattice distortions under strain.[13] Hence, it is imperative to study the electromechanical response of this type of materials.

Here, using DFT calculations, we systemically investigate the stability, electronic and magnetic properties of 2D α-Fe_2O_3 sheets and their functionalized derivatives. We show that, depending on chemical termination, Hm can be an indirect-band gap magnetic semiconductor, magnetic half-metal or magnetic metal. Specifically, the fully hydrogenated monolayer is a ferromagnetic semiconductor, while the bare sheets are antiferromagnets, with a smaller band gap as compared to that in the passivated monolayer. The effects of external strain are also examined. Our findings indicate that the electronic structure of Hm can effectively be engineered by applying external strain. In particular, the band gap in both bare and passivated Hm changes under biaxial strain.

2. COMPUTATIONAL METHOD

Spin-polarized density functional theory (DFT) calculations were performed using the generalized gradient approximation (GGA) with the Perdew-Burke-Ernzerhof (PBE) parametrization for the exchange-correlation (XC) functional as implemented in the VASP code.[14–16] The effects of the Coulomb repulsion of the 3d localized electrons of iron atoms in oxide systems are not well described in the DFT. Therefore, we performed DFT+U calculations (Hubbard-type on-site Coulomb repulsion) to account in part for the local correlation effects that regular XC functionals fail to represent. An effective Hubbard value (U_{eff}) of 4 eV was chosen for Fe atoms by comparing the band gap values of bulk α-Fe_2O_3 with the experimental one.[17,18] Thus, the U_{eff} value and lattice parameter from this magnetic ground state will be employed for all calculations. For all other atoms, the Hubbard term was not used. Projected augmented plane wave (PAW) potentials were used to represent the frozen core electrons and nuclei of each atom: [Ar] $3d^6$ $4s^2$ shells in Fe atoms, [He] $2s^2 2p^4$ shells in O atoms. All the calculations were performed using an energy cutoff of 550 eV. The Brillouin zone of the supercells was sampled using a 8 × 8 × 8 *k*-

point mesh for bulk and 15 × 15 × 1 for monolayer according to the scheme proposed by Monkhorst and Pack.[19] The geometry optimization was carried out until the atomic forces were less than 0.01 eV/Å. In order to avoid the interactions between neighboring images, a vacuum of 20 Å was introduced perpendicular to the basal plane. The exfoliation energy $E_{exfoliation}$ of a bulk phase into 2D slab is defined as

$$E_{exfoliation} = [E_{slab} - E_{bulk}]/2A$$

where E_{slab}, E_{bulk} stand for the total energies (per formula unit) of bulk and 2D slab, respectively. A represents the surface area. The energetics of the passivated surface was evaluated as

$$E_{absorption} = E_{passivated} - E_{bare} - n\mu_O - m\mu_H ,$$

where $E_{passivated}$ and E_{bare} are the total energies of Hm with and without passivation, *n* and *m* are the numbers of additional oxygen and hydrogen atoms on the surface, μ_O and μ_H are the chemical potentials of oxygen and hydrogen.

3. RESULTS AND DISCUSSION

3.1 Geometric structures and stabilities

The initial (before geometry optimization) atomic structure of a Hm sheet was truncated directly from the bulk hematite. As it is indicated in the previous experimental study, the [001] faceted α-Fe_2O_3 sheet is the most stable and thermodynamically favorable configuration.[4] Besides, Fe-terminated hematite surface, containing half of the interplane Fe atoms, is more stable than those of the O-terminated surface in a wide range of oxygen chemical potential values.[17] Therefore, we have studied the energetics of Fe-terminated [001] Hm from both ferromagnetic (FM) and antiferromagnetic (AFM) alignment of the spins. Our calculations suggest that AFM is the ground

state configuration being lower by 0.14 eV (per formula unit) in energy as compared to the FM state.

We stress that when we use terms "FM" and "AFM Hm", we refer to different spin configurations in our calculations, and no strict conclusion on the long-ranged magnetic state of the macroscopic 2D sample can be made. Non-collinear calculations with magnetic moments parallel and perpendicular to the Hm plane can help to get insight into the true nature of magnetism in 2D systems [Phys. Rev. B 101, 205425, and 2D Mater. 4 035002], but such calculations are computationally demanding and require high accuracy. Our non-collinear test calculations with account for spin-orbit coupling in the FM configurations with the magnetic moments parallel and perpendicular to plane for Hm-H and Hm-OH gave very close results (with a difference of the order of 0.01 eV), so that within our accuracy, no decisive conclusion on the existence of the long-range FM order in the passivated Hm can be made.

The in-plane lattice parameters are found to be $a=b=5.17$ Å in the most stable AFM configuration, which is slightly larger (2.5%) than that of the experimental lattice parameters of 5.04 Å[4] and in a very good agreement with the recent DFT report.[20] The thickness of the relaxed sheet, which we refer to as a monolayer is found to be 3.02 Å matching very well with the previous report [4]. Table S1 summarizes the optimized lattice parameters for bulk and 2D structures.

To mimic the effects of different environmental conditions, we investigate the passivation of Hm with two species including hydrogen (H) and hydroxyl (OH). Due to the presence of the Fe and O on the surface of Hm, we consider two possibilities for passivation: half coverage: only the outmost Fe surface atoms are covered with the H/OH groups. Full coverage: all Fe and O atoms are covered with the H/OH groups. Figure 1 demonstrates the relaxed structures of bare and passivated-Hm monolayers. In order to analyze the structural stability of the chemically passivated

Hm, we calculated the absorption energy as a function of μ_O in Figure 2. The results demonstrate that Hm with full OH passivation is energetically favorable over the whole range of the considered μ_O values. The half OH passivated Hm, with higher formation energies than fully passivated one, adopts the same tendency with respect to the O chemical potential. Meanwhile, the stoichiometric H passivated slabs are more stable than the half OH passivated surface under oxygen-poor conditions. Our formation energies are in a good agreement with earlier computational reports indicating that the surface may be partially or completely reoxidized by raising the oxygen chemical potential i.e. pressure.[21,22]

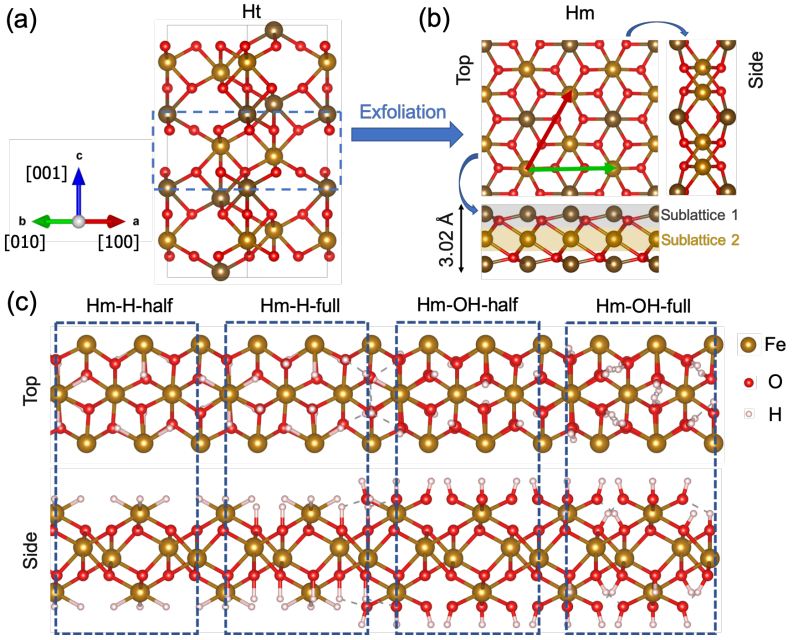

Figure 1. (a) Atomic structure of bulk hematite (Ht) and (b) schematic of its exfoliation into hematene (Hm). The thickness of Hm is outlined by the blue dashed line in panel. Brown and red balls represent Fe and O atoms. Light and dark brown colors correspond to the Fe atoms from inner (1) and outer (2) sublattices, respectively. (c) Atomic structure of Hm with different passivation with H and OH groups.

Table 1. The magnetic properties of hematene with and without passivation. The energy difference $\Delta E = E_{AFM} - E_{FM}$ and average magnetic moments per Fe atoms are given (μ_{Fe}) in eV/formula unit and μ_B, respectively. Sublattice labels as in Figure 1.

Material	Hm	Hm-H-half	Hm-H-full	Hm-OH-half	Hm-OH-full
ΔE	-0.55	-0.15	0.48	0.11	-0.11
μ_{Fe}^{sub1}(AFM/FM)	4.17/4.35	3.77/3.90	4.11/3.79	3.93/3.39	4.27/4.31
μ_{Fe}^{sub2}(AFM/FM)	3.99/4.17	2.97/3.05	3.86/2.39	0.58/4.11	4.21/4.24
μ_{Fe}^{total}(AFM/FM)	4.08/4.26	3.37/3.48	3.98/3.09	2.25/3.75	4.24/4.28

Table 1 lists the energy difference $\Delta E = E_{AFM} - E_{FM}$ for various surface passivations, where E_{AFM} and E_{FM} represent the total energies of the AFM and FM configurations, respectively. The passivation can considerably affect the structural and magnetic properties of the monolayer. The Hm-H-half is more stable (by 0.15 eV per formula) in the AFM state than in the FM state, while Hm-H-full prefers to stay in the FM state. The trend changes in the case of Hm-OH. Although Hm-OH-half prefers to exist in FM configuration, Hm-OH-full is more stable in the FM state. However, the difference between the FM and AFM states in Hm-OH is less pronounced in comparison to the Hm-H (only 0.11 eV per formula). Besides the stability differences, the passivation can lead to magnetization diversity, as shown in Table 1. In general, the average value of the calculated moments for inner Fe atoms (μ_{Fe}^{sub1}) is larger than those for outer Fe atoms (μ_{Fe}^{sub2}). This is due to the specific chemical environment of the atoms in the outer layers, i.e. coordination with regard to the surrounding atoms, which causes a deviation of magnetic moments from the bulk values (~4 μ_B). The iron atoms in bare Hm demonstrate higher magnetic moments in the FM states, which is slightly higher than those in bulk Ht (4.16 μ_B). The passivation of the surface, in particular, iron atoms, reduces the magnetization and the lowest value (2.25 μ_B) was obtained for

the Hm-OH-half configuration in the AFM state. Interestingly, the full passivation with the hydroxyl group will not significantly change the magnetic moments of iron atoms and the values are similar to those for bare Hm.

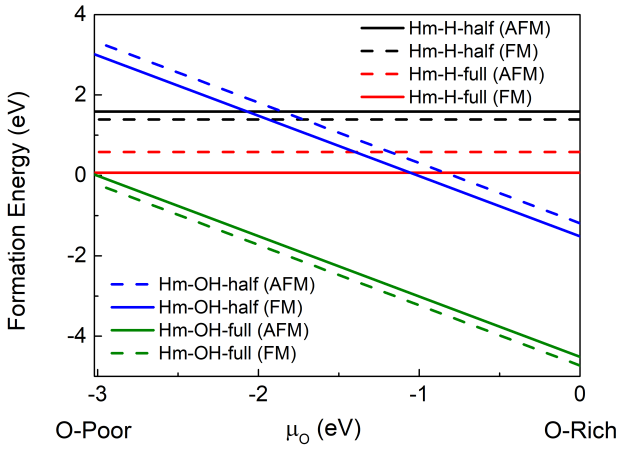

Figure 2. Calculated formation energies of the Hm with various passivations as functions of the chemical potential for the O-atoms. The solid and dashed lines denote the structures in the AFM and FM magnetic states.

3.2 Electronic and magnetic properties

The electronic structure of the material is significantly modified by confining the bulk material to the monolayer. Hematite shows a band gap of 2.16 eV, which originates from a transition from the valence band maxima (VBM) situated at *M* point to the conduction band minima (CBM) halfway between *M* and *K* points (see Figure S1). Our results are in perfect agreement with the other theoretical works reported at a similar level of theory and match the experimental band gap, which is in the range of 1.9-2.2 eV.[18,23–25] The exfoliation of Ht to Hm leads to emerging confined electronic states and consequently the monolayer has a smaller band gap than the bulk material (Figure 3 a,b). In the most stable AFM configuration, the Hm shows an indirect band gap of 0.93

eV occurring from the *K*-*Γ* transition. The shape of the electronic structure and the band gap for bare Hm are in good agreement with the previous theoretical works.[5,9]

The character of the low energy bands has been investigated using the crystal orbital Hamilton population (COHP)[26]. The COHP is computed by applying the results of the density of states matrix to the Hamilton matrix. The negative and positive values of COHP reflect the antibonding and bonding character of orbitals. It is found that while the top of the valence band and bottom of the conduction band are bonding type in AFM state, their corresponding orbitals have antibonding character in FM state.

The orbital-projected densities of state (Figure 3 c,d) suggest that the top of the valence band is composed of fully occupied O $2p_{x,y}$ orbitals, while the edge of the conduction band is mainly formed by the Fe $3d_{z2}$ orbitals and slight contributions from O $2p_z$ states. Because of its low dispersion, this band may trap charge carriers localized on the surface. The next delocalized states are present only at about ~0.93 eV above the Fermi level, consistent with the previous report.[5] In the case of the FM state, the electronic structure changes even stronger with a larger number of midgap states that reduce the band gap to 0.6 eV. Further analyses by atom- and orbital-decomposed band structure showed that the CBM originates from spin down components of mainly Fe atoms (Figure S2). Besides, the VBM at the *K* point (AFM state) is only formed by spin down states from O atoms, while the VBM at the *Γ* point (FM state) is composed of spin up states.

Figure 4a shows the impact of the confinement on the electronic band gap of the slabs. Due to the relatively high stability of multilayers, only the AFM state is taken into consideration. Contrary to the Gaussian smearing method employed in ref 20, we have used a more accurate tetrahedron method to calculate occupancies of the states around the Fermi level which does not depend on the smearing parameter.[20]

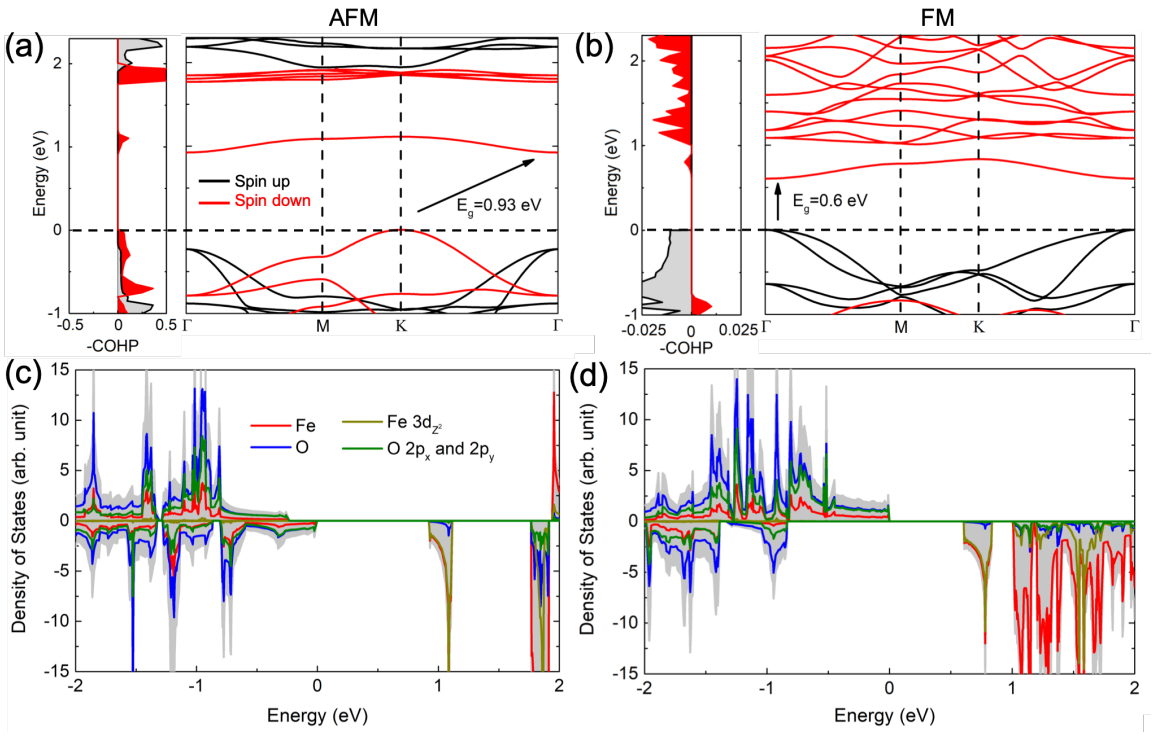

Figure 3. Calculated electronic band structure and crystal orbital Hamiltonian population (COHP) of Hm in (a) the AFM and (b) FM configurations. Red and black lines denote spin up and spin down contributions, respectively. Density of states of Hm in the AFM (c) and FM (d) states. The Fermi level is shifted to zero. The projections on Fe and O atoms are shown by red and blue colors, respectively. The gray corresponds to the total density of states.

It is found that the band gap increases with slab thickness from monolayer to bilayer slab (~7 Å), and remains almost constant by further extending the system size. The trend is related to the electronic states caused by under-coordinated surface atoms which induce weak convergence in the band gap values as a function of the slab thickness. Our results for the thickness-dependent electronic properties of α-Fe_2O_3 proved to be in agreement with those presented in the reference.[5] The surface states in multilayer Hm are found to be localized on the three top-most Fe layers and substantially suppressed for the innermost part of the slab (Figure 4 b). In addition, the lattice

parameters are found to decrease slowly with the thickness of the slabs, converging to those of bulk (Figure S3).

The passivation can effectively change the electronic and magnetic properties of Hm (Figure 5). Upon passivation of the surface with hydrogen, in both half and full coverage in FM configuration, the monolayer becomes half-metal, i.e., the states at the Fermi level are entirely from one type of the spin band, while the full coverage in AFM configuration has a band gap of 0.16 eV. The emergence of the half-metallic character is associated with the splitting between the majority and minority spin subbands in the vicinity of the Fermi level. For Hm-H-half in most stable AFM configuration, the electronic structure at the Fermi level is dominated by O*p* spin down states while those in Hm-H-full are originated from Fe *d* spin-down orbitals (Figure S4).

From Figure 6, the increment of both Fe *d* states and O *p* states around the Fermi level suggests a strong Fe-O hybridization in the Hm-H-full configuration. As a result, the magnetic moment for outmost Fe atoms decreases in comparison to the bare Hm (Table 1). In addition, the difference between two spin components of Fe 3d orbitals reduces when the magnetic state is changed from AFM to FM. This leads to a deduction of the magnetic moment of Fe atoms. In the case of the OH passivation, the average Fe-O bonds are shorter than that of the hydrogen passivation which changes the valence state of Fe ions and increases the iron magnetic moments.

In order to identify the origin of the magnetism, the charge density difference between the spin-up and spin-down channels ($\Delta\rho = \rho^{\uparrow} - \rho^{\downarrow}$) was calculated. The two magnetic configurations show different $\Delta\rho$ characteristics: the polarization of the electron spin for the surface iron atoms and the central oxygen atoms is similar for the FM configuration, while they have different polarization for the AFM configuration. The real space projections indicate a *d*-like orbital located at the Fe atoms in both outer and inner layers, which is in agreement with the corresponding DOS. In

addition, spin polarization on hydrogen atoms is more pronounced in the FM than the AFM configuration.

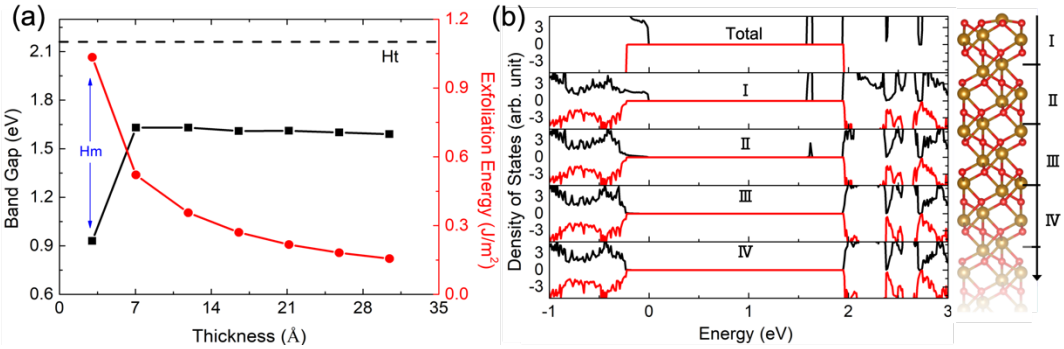

Figure 4. (a) Band gap values and exfoliation energy of α-Fe_2O_3 as functions of slab thickness. The horizontal dashed lines indicate the band gap of the bulk material. (b) Local density of states of α-Fe_2O_3 slab in different areas of the surface.

In the most stable FM state, the spin up band arises primarily from the 3*d* orbitals of the Fe atoms, in addition to a slight contribution from the 2*p* orbitals of the O atoms. The stability of fully passivated Hm can be explained by the Goodenough-Kanamori rule.[27,28] The overlap between Fe atoms with the *p* orbitals of O leads to super-exchange interaction, which is stronger than the direct exchange interaction between nearest-neighbor Fe atoms. In bare Hm, the magnetic interaction between outer Fe_2 atoms is associated with the direct exchange mechanism. Although the distance between Fe_1 atoms is large, the Coulomb repulsion decays as rapidly as the hopping power giving rise to AFM coupling. On the other hand, the Fe_1–Fe_1 and the Fe_1–Fe_2 interactions are mediated by O atoms via a super-exchange mechanism. The coupling strength between the partly occupied Fe *d* and O *p* orbitals changes with the passivation. Hm demonstrates FM coupling when super-exchange interaction is stronger than direct exchange interaction, otherwise it displays AFM

coupling. The full passivation with H reduces the direct exchange between Fe_2 atoms (see Table 1) leading to dominant FM interaction in the system.

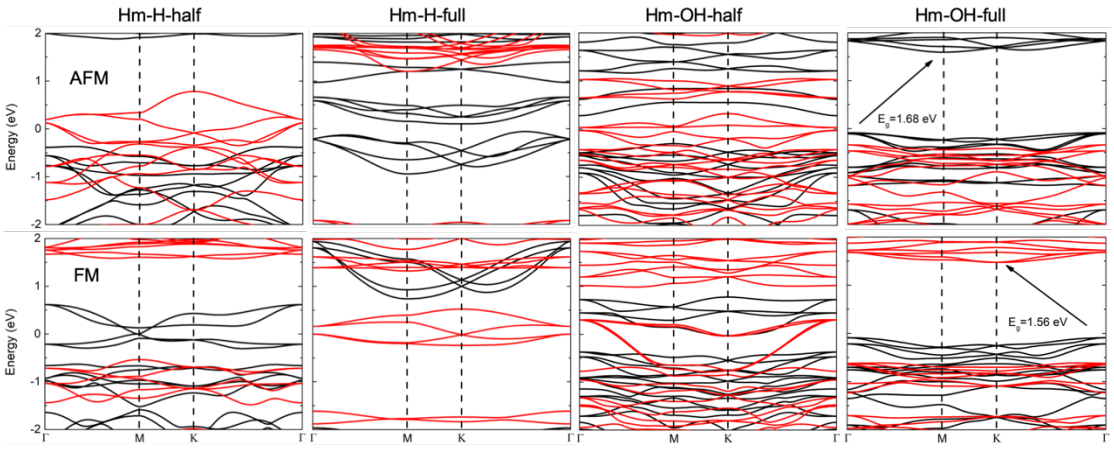

Figure 5. Calculated electronic band structure of Hm with different passivation in the AFM (upper panels) and FM (lower panels) states. Spin up and spin down electronic states are shown with black and red lines, respectively. The Fermi level is shifted to zero.

Similar half-metallic behavior can be seen in the case of Hm-OH-half although the partial hybridization of the surface states with hydroxyl group delocalizes the states above the Fermi level. Notably, surface states that were seen on bare hematene are absent in fully passivated Hm with hydroxyl groups. The effect of the OH coverage is twofold. First, it passivates the Fe-d_{z2} states at the Hm surface and consequently increases the band gap to 1.68 eV and 1.56 eV for AFM and FM magnetic states. Second, the shape of the bottom of the conduction band changes from AFM to FM state with a shift of the CBM from *M* to *K* point.

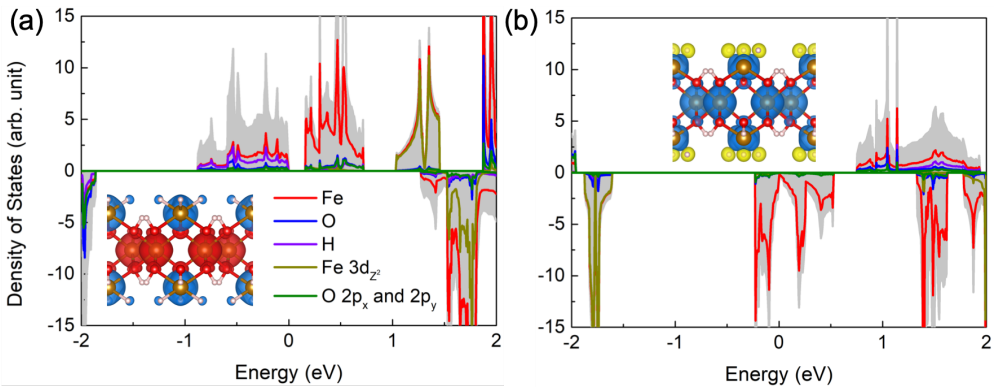

Figure 6. Density of states for Hm-H-full in (a) the AFM and (b) FM magnetic states. The contribution of Fe, O and H atoms are shown by red, blue, and purple colors, respectively. The gray indicates the total density of states. The insets show the density difference between the spin-up and spin-down states.

3.3 Effect of mechanical deformations

The remarkable degrees of tunability in 2D crystals motivates their applications in the field 'straintronics' suggesting electronic devices that are engineered by mechanical deformations.[29] Here, the structures are subjected to tensile and compressive strain (ε) following two possible ways: (1) isotropic deformation on the hexagonal unit cells with simultaneous change of the *a* and *b* lattice vectors, (2) uniaxial deformation in rectangular unit cells along *a* or *b* directions. The calculated stress-strain relation curves, which display linear scaling throughout the range of strain, indicate compliance of Hooke's law (Figure 7). We note that the structural modifications due to the applied deformations are elastic, and the material will return to their equilibrium structure after the release of the strain. The corresponding elastic modulus is defined by fitting the linear function with the stress-strain curve. Based on the calculations, Hm shows an elastic modulus (Y_ε) of 234 GPa and 232 GPa along the a and b lattice vectors, respectively. These values are close to the

experimental Young's modulus of 230±5 GPa reported for bulk hematite and higher than those for single-layer transition metal dichalcogenides.[13,24]

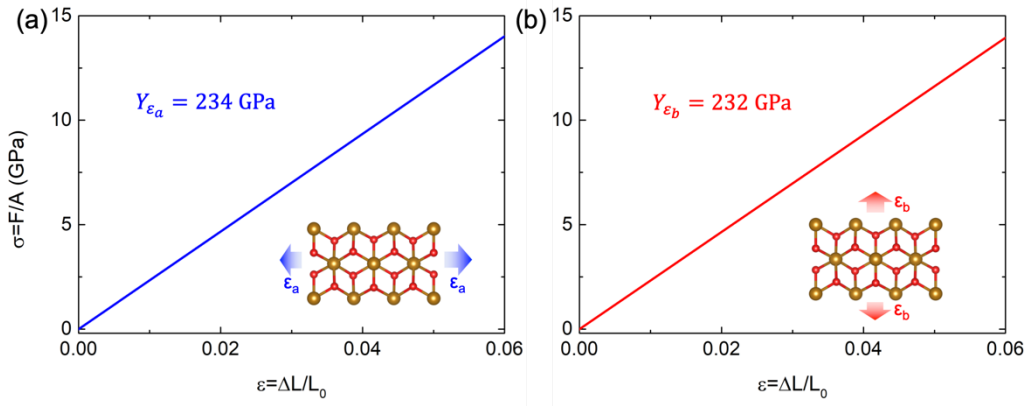

Figure 7. Calculated strain-stress relation for Hm in AFM state along the *a* (a) and *b* (b) lattice vectors. The Young's moduli for the deformations are indicated by Y_{ε_a} and Y_{ε_b}. The insets indicate the directions of the strain.

Tensile strain and compression can cause structural adjustments in the material, including expansion or shrinkage of bond lengths and angles. Figure 8 a,b illustrates the modulation of interatomic distances and the bond angles in Hm under the applied strain. The equilibrium bond lengths are 1.82 Å (Fe_1-O) and 2.02 Å (Fe_2-O) which are similar to the previously reported values 9. Owning to the Poisson effect, the biaxial stretching of the material leads to its contraction in the transverse direction. Both bond lengths rise by approximately 0.01 Å per 1% of isotropic tensile strain. At the same time, the O-Fe_2-O bond angle is decreased by ~1.1° per 1% of isotropic tensile strain. The variation of bond lengths and angles is almost linear with the applied deformation for the strain up to about 6%. The geometry modifications in Hm are very similar in both AFM and AFM magnetic states for a given strain.

Changes in the atomic structure of the monolayers modify the orbital overlap between atoms that influence the charge distribution in these materials (Figure 8 c). We have studied the evolution of the atomic charges for both Fe and O atoms using the Mulliken charge analysis. The tensile strain reduces the electron charge on iron atoms, while it causes accumulation of charges on oxygen atoms. This suggests that the Fe-O bond in the strained material is more ionic in comparison with the equilibrium structure. Similarly, in fully passivated Hm surfaces with the OH group, the iron atoms become more positive with increasing tensile strain, while hydrogen receives more electrons under deformation (Figure S5).

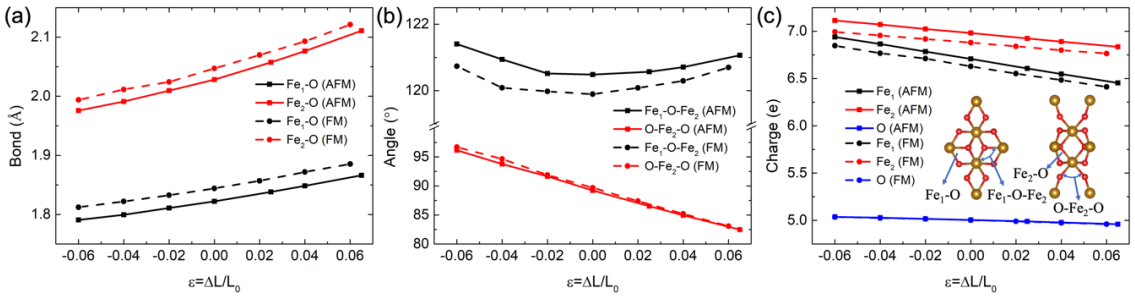

Figure 8. Calculated (a) Fe-O bond lengths, (b) O-Fe-O bond angles, and (c) atomic charges of Hm under tensile strain and compression. The solid and dashed lines denote the structures in the AFM and FM states. The inset shows the top and side views of the system.

The evolution of band gap with the biaxial strain for Hm is shown in Figure 9. Under biaxial tensile strain, the band gap of Hm in the AFM state decreases. Similar behavior is observed for the monolayer under the uniaxial strain (Figure S6), although the influence is smaller than that of the biaxial tensile strain. Unlike the AFM state, the band gap in the FM state grows up with increasing tensile strain, while the band gap remains direct at the *Γ* point. It can be seen that both the VBM and CBM shift up with increasing tensile strain, while the behaviour is opposite under the compressive strain (Figures S7 and S8). The modulation of the band gap with the in-plane

deformations hints at the possible use of Hm in strain-tunable infrared devices as previously suggested for phosphorene or silicene.[30,31] We further studied the strain dependence of the magnetic moments of iron atoms. The average magnetic moment of Fe atoms in the AFM state first decreases and then increases slightly with strain from -6 to 6%. In contrast, the Fe magnetic moments in the FM state increases monotonically within the applied strain.

The electromechanical response of Hm is greatly influenced by the surface morphology. Since we are interested in the band gap modulation with the applied strain, the fully OH passivated Hm with the semiconducting character was chosen. Unlike bare Hm, tensile strain linearly increases band gap of the fully OH passivated Hm in both the FM and AFM states (Figures S9 and S10). At 6 % elongation, band gap accounts for more than 15% of its original value. Within the deformation, the band gap remains indirect with a transition from the Γ to *M* and *K* high symmetry points for AFM and FM configurations. As compared with Hm, the energy of the valence band at the *M* and *K* point does not show noticeable increment under tensile strain, whereas the energy difference between CBM and the *M* point dramatically decreases under tensile strain for FM configuration (Figure S10). The charge analyses indicate that hydrogen atoms receive more charges under the deformation while the charge on iron atoms slightly reduces with the increase of the strain (Figure S8). Moreover, the magnetic moment of Hm-OH-full in both magnetic states change only ~0.5% over -6%-6% of strain (Figure S11).

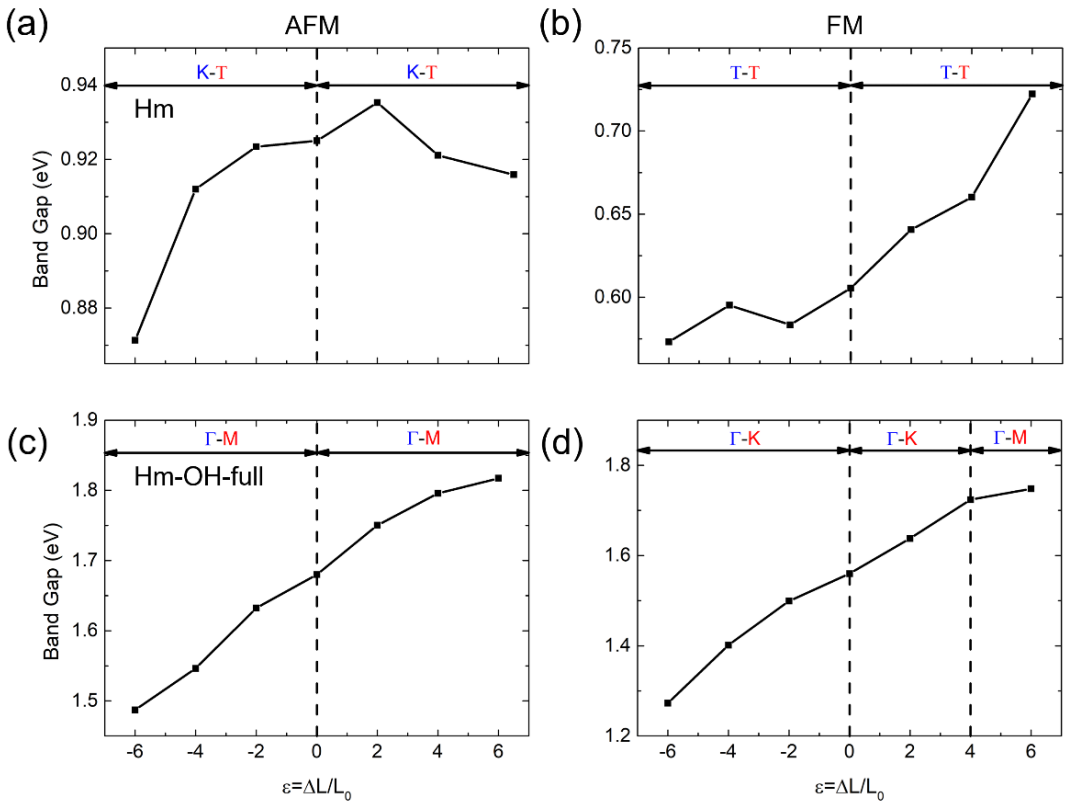

Figure 9. Band gap evolution of Hm (a,b) and Hm-OH-full (c,d) under isotropic tensile strain and compression. The *k* points, at which the top of valence band and the bottom of conduction band occur, are indicated.

4. CONCLUSIONS

In summary, we systematically studied the effects of surface morphology and strain on the electronic and magnetic properties of Hm. In the most stable AFM configurations, bare Hm is an indirect band gap semiconductor with a smaller band gap in comparison to its bulk counterpart. The band gap of the exfoliated slab increases with the thickness from monolayer to the bilayer, while the exfoliation energy decreases. Motivated by high surface reactivity of Hm, several types of surface passivation with H and OH groups have been taken into consideration. The results suggest that the surfaces passivated with OH groups are energetically favored over a wide range

of oxygen chemical potential. The electronic and magnetic properties of Hm are sensitive to the surface passivation and can be tuned depending on the type and coverage of the H/OH groups. Interestingly, the hydrogenated sheets are found to be a half-metal with a ferromagnetic ground state, whereas the fully hydroxylated sheets are antiferromagnetic semiconductors. Under 2D-isotropic strain, the electronic band gap of bare Hm decreases in the AFM configuration, while the effect is opposite in the FM configuration. In addition, the band gap of fully hydroxylated Hm monotonically increases under applied strain. Our research indicates that surface passivation and mechanical deformations can be an effective tool to modulate the electronic and magnetic properties of this novel 2D system and possibly other non-vdW 2D materials.

ASSOCIATED CONTENT

Supporting Information

The Supporting Information is available free of charge on the ACS Publications website.

AUTHOR INFORMATION

Corresponding Author

Mahdi Ghorbani-Asl - Institute of Ion Beam Physics and Materials Research, Helmholtz Zentrum Dresden Rossendorf, Dresden 01328, Germany.

Email: mahdi.ghorbani@hzdr.de

Arkady V. Krasheninnikov - Institute of Ion Beam Physics and Materials Research, Helmholtz Zentrum Dresden Rossendorf, Dresden 01328, Germany; Department of Applied Physics, Aalto University, P.O. Box 11100, 00076 Aalto, Finland.

Email: a.krasheninnikov@hzdr.de

Authors

Yidan Wei - Institute of Ion Beam Physics and Materials Research, Helmholtz Zentrum Dresden Rossendorf, Dresden 01328, Germany.

Notes

The authors declare no competing financial interest.

ACKNOWLEDGMENT

The authors thank the HZDR computing center, PRACE (HLRS, Stuttgart, Germany, Project ID: 2018184458), and TU Dresden Cluster "Taurus" for generous grants of CPU time. A.V. K. acknowledges financial support from the DFG, project KR 4866/2-1. Y. Wei thanks the financial support by Chinese Scholarship Council (File No. 201806120150).

REFERENCES

(1) Chhowalla, M.; Shin, H. S.; Eda, G.; et al. The Chemistry of Two-Dimensional Layered Transition Metal Dichalcogenide Nanosheets. Nat. Chem. 2013, 5 (4), 263–275.

(2) Novoselov, K. S.; Jiang, D.; Schedin, F.; et al. Two-Dimensional Atomic Crystals. Proc. Natl. Acad. Sci. 2005, 102 (30), 10451–10453.

(3) Coleman, J. N.; Lotya, M.; O'Neill, A.; et al. Two-Dimensional Nanosheets Produced by Liquid Exfoliation of Layered Materials. Science 2011, 331 (6017), 568–571.

(4) Puthirath Balan, A.; Radhakrishnan, S.; Woellner, C. F.; et al. Exfoliation of a Non-van Der Waals Material from Iron Ore Hematite. Nat. Nanotechnol. 2018, 13 (7), 602–609.

(5) Padilha, A. C. M.; Soares, M.; Leite, E. R.; et al. Theoretical and Experimental Investigation of 2D Hematite. J. Phys. Chem. C 2019, 123 (26), 16359–16365.

(6) Puthirath Balan, A.; Radhakrishnan, S.; Kumar, R.; et al. A Non-van Der Waals Two-Dimensional Material from Natural Titanium Mineral Ore Ilmenite. Chem. Mater. 2018, 30 (17), 5923–5931.

(7) Liu, S.; Xie, L.; Qian, H.; et al. Facile Preparation of Novel and Active 2D Nanosheets from Non-Layered and Traditionally Non-Exfoliable Earth-Abundant Materials. J. Mater. Chem. A 2019, 7 (25), 15411–15419.

(8) Gong, C.; Li, L.; Li, Z.; et al. Discovery of Intrinsic Ferromagnetism in Two-Dimensional van Der Waals Crystals. Nature 2017, 546 (7657), 265–269.

(9) Gonzalez, R. I.; Mella, J.; Díaz, P.; et al. Hematene: A 2D Magnetic Material in van Der Waals or Non-van Der Waals Heterostructures. 2D Mater. 2019, 6 (4), 045002.

(10) Butler, S. Z.; Hollen, S. M.; Cao, L.; et al. Progress, Challenges, and Opportunities in Two-Dimensional Materials Beyond Graphene. ACS Nano 2013, 7 (4), 2898–2926.

(11) Mohanty, B.; Wei, Y.; Ghorbani-Asl, M.; et al. Revealing the Defect-Dominated Oxygen Evolution Activity of Hematene. J. Mater. Chem. A 2020, 8 (14), 6709–6716.

(12) Li, Q.; Zhou, Q.; Shi, L.; et al. Recent Advances in Oxidation and Degradation Mechanisms of Ultrathin 2D Materials under Ambient Conditions and Their Passivation Strategies. J. Mater. Chem. A 2019, 7 (9), 4291–4312.

(13) Ghorbani-Asl, M.; Borini, S.; Kuc, A.; et al. Strain-Dependent Modulation of Conductivity in Single-Layer Transition-Metal Dichalcogenides. Phys. Rev. B 2013, 87 (23), 235434.

(14) Perdew, J. P.; Burke, K.; Ernzerhof, M. Generalized Gradient Approximation Made Simple. Phys. Rev. Lett. 1996, 77 (18), 3865.

(15) Kresse, G.; Hafner, J. Ab Initio Molecular Dynamics for Liquid Metals. Phys. Rev. B 1993, 47 (1), 558–561.

(16) Kresse, G.; Furthmüller, J. Efficiency of Ab-Initio Total Energy Calculations for Metals and Semiconductors Using a Plane-Wave Basis Set. Comput. Mater. Sci. 1996, 6 (1), 15–50.

(17) Rohrbach, A.; Hafner, J.; Kresse, G. Ab Initio Study of the (0001) Surfaces of Hematite and Chromia: Influence of Strong Electronic Correlations. Phys. Rev. B 2004, 70 (12), 125426.

(18) Ingler Jr, W. B.; Khan, S. U. . Photoresponse of Spray Pyrolytically Synthesized Magnesium-Doped Iron (III) Oxide (p-Fe2O3) Thin Films under Solar Simulated Light Illumination. Thin Solid Films 2004, 461 (2), 301–308.

(19) Monkhorst, H. J.; Pack, J. D. Special Points for Brillouin-Zone Integrations. Phys. Rev. B 1976, 13 (12), 5188–5192.

(20) Bacaksiz, C.; Yagmurcukardes, M.; Peeters, F. M.; et al. Hematite at Its Thinnest Limit. 2D Mater. 2020, 7 (2), 025029.

(21) Parkinson, G. S. Iron Oxide Surfaces. Surf. Sci. Rep. 2016, 71 (1), 272–365.

(22) Diebold, U.; Li, S.-C.; Schmid, M. Oxide Surface Science. Annu. Rev. Phys. Chem. 2010, 61 (1), 129–148.

(23) Nakau, T. Electrical Conductivity of α-Fe 2 O 3. J. Phys. Soc. Japan 1960, 15 (4), 727–727.

(24) Glasscock, J. A.; Barnes, P. R. F.; Plumb, I. C.; et al. Structural, Optical and Electrical Properties of Undoped Polycrystalline Hematite Thin Films Produced Using Filtered Arc Deposition. Thin Solid Films 2008, 516 (8), 1716–1724.

(25) Sivula, K.; Zboril, R.; Le Formal, F.; et al. Photoelectrochemical Water Splitting with Mesoporous Hematite Prepared by a Solution-Based Colloidal Approach. J. Am. Chem. Soc. 2010, 132 (21), 7436–7444.

(26) V. L. Deringer, A. L. Tchougréeff, and R. Dronskowski, Crystal Orbital Hamilton Population (COHP) Analysis As Projected from Plane-Wave Basis Sets, J. Phys. Chem. A 2011, 115, 21, 5461–5466

(27) Kanamori, J. Crystal Distortion in Magnetic Compounds. J. Appl. Phys. 1960, 31 (5), S14–S23.

(28) Goodenough, J. B. Theory of the Role of Covalence in the Perovskite-Type Manganites [La,M(II)] MnO3. Phys. Rev. 1955, 100 (2), 564–573.

(29) Novoselov, K. S.; Castro Neto, A. H. Two-Dimensional Crystals-Based Heterostructures: Materials with Tailored Properties. Phys. Scr. 2012, T146 (T146), 014006.

(30) Tran, V.; Yang, L. Scaling Laws for the Band Gap and Optical Response of Phosphorene Nanoribbons. Phys. Rev. B 2014, 89 (24), 245407.

(31) Kim, J.; Fischetti, M. V; Aboud, S. Structural, Electronic, and Transport Properties of Silicane Nanoribbons. Phys. Rev. B 2012, 86 (20), 205323.

Graphical abstract

The surface passivation modulates the stability, electronic, and magnetic properties of Hematene and leads to an antiferromagnetic-ferromagnetic transition, providing an excellent opportunity to realize spintronics at the atomically thin single-layer crystals.